https://doi.org/10.5194/egusphere-2026-1143
Preprint. Discussion started: 6 March 2026


# Soil–atmosphere water vapor exchange in semi-arid Northwest China: New insights from fiber-optic relative humidity sensing

Junyi Guo[1], Mengya Sun[2], Chengcheng Zhang[1], Jie Liu[3], Qingnan Lou[1], Qiyu Xu[1], and Bin Shi[1]

[1]School of Earth Sciences and Engineering, Nanjing University, Nanjing, 210023, China
[2]School of Earth Sciences and Engineering, Hohai University, Nanjing, 210023, China
[3]Huairou Laboratory, Beijing, China

*Correspondence to*: Bin Shi (shibin@nju.edu.cn)

**Abstract.** Soil–atmosphere water vapor exchange in arid and semi-arid regions is a key process in near-surface hydrology, reflecting the dynamic coupling of surface energy and moisture. In this study, a novel fiber-optic sensing technique was employed to measure vertical water vapor fluxes across the soil–atmosphere interface in a semi-arid region of the Loess Plateau, Yanan, China. The observations captured vapor flux dynamics across a 7-mm dry soil layer beneath the interface (hereafter referred to as Flux Layer $_{soil}$) and a 10-mm molecular diffusion layer in the air above it (Flux Layer $_{air}$), revealing how meteorological factors modulate near-surface vapor transport. Solar radiation enhanced vapor fluxes primarily by increasing the vapor pressure deficit (VPD), with Flux Layer $_{soil}$ exhibiting a slower response than Flux Layer $_{air}$. This lag was most pronounced in winter, reaching up to 120 minutes. During rainfall, fluxes in both layers declined sharply as VPD dropped to near zero. Following precipitation, Flux Layer $_{air}$ recovered rapidly, driven by surface evaporation, while Flux Layer $_{soil}$ increased more gradually due to the progressive drying of subsurface moisture. Structural equation modeling based on 5657 observations revealed distinct influence pathways: Flux Layer $_{air}$ was more sensitive to solar radiation, air temperature, and VPD, while Flux Layer $_{soil}$ was predominantly governed by VPD. These findings advance the quantitative understanding of near-surface vapor transport mechanisms and improve insight into the coupled feedbacks governing soil–atmosphere interactions under variable climatic conditions.

## 1 Introduction

The soil–atmosphere interface serves as a critical boundary for the exchange of heat and water between the underlying soil and the overlying atmosphere (Humphrey et al., 2021; Phillips et al., 2017). In arid and semi-arid regions, a steep vapor gradient commonly develops between the dry soil layer (DSL) beneath the interface and the molecular diffusion layer in the air above, driving vapor transport across this narrow transition zone (Du et al., 2018; McHugh et al., 2015). This exchange demonstrates substantial temporal variability and physical complexity, primarily governed by meteorological factors such as net radiation, air temperature, relative humidity, and episodic rainfall events (Gu et al., 2006; Meng et al., 2017). Accurately quantifying vertical water vapor fluxes across the narrow transition zone surrounding the soil–atmosphere interface—together with a mechanistic understanding of their meteorological drivers—is essential for advancing boundary layer representations in land–

https://doi.org/10.5194/egusphere-2026-1143
Preprint. Discussion started: 6 March 2026


atmosphere models, particularly in dryland regions where surface feedbacks strongly modulate regional climate dynamics (Bagley et al., 2017; Wang et al., 2024; Yan et al., 2020).

Soil water evaporation is a major source of atmospheric moisture in arid and semi-arid regions and plays a pivotal role in regulating the magnitude and variability of near-surface vapor fluxes (Lehmann et al., 2012; Wang et al., 2010). Using the eddy covariance technique, Liu et al. (2022) measured vertical vapor fluxes from the surface up to 2.7 m and observed consistent diurnal cycles with peak values typically around 14:00, primarily controlled by air temperature, evapotranspiration, and vapor pressure deficit (VPD). In tropical rice fields during the dry season, Chatterjee et al. (2019) found that vapor fluxes within the 0–1.5 m layer were jointly modulated by latent heat flux, net radiation, and the thermal regimes of both air and soil. While these studies provide valuable insights into vapor transport at the meter scale within the atmospheric boundary layer, they largely neglect the millimeter-scale molecular sublayer immediately above the land surface (Choi et al., 2004). This ultra-thin layer—characterized by near-zero wind speed and turbulence suppression due to surface friction—is dominated by molecular diffusion rather than turbulent mixing, rendering traditional eddy covariance methods ineffective (Fetzer et al., 2017). Despite its shallow depth, the molecular sublayer serves as the initial interface for mass and energy exchange and plays a critical role in shaping evaporation dynamics, soil–atmosphere coupling, and near-surface atmospheric stability (Shahraeeni et al., 2012).

In arid and semi-arid regions, prolonged water scarcity often results in the formation of a near-surface DSL, characterized by dominant vapor-phase transport and sustained exchange with the overlying atmosphere (Shokri et al., 2009; Weiss et al., 2018). Previous studies have demonstrated that vapor fluxes in this zone can be comparable in magnitude to liquid water fluxes and exert a significant influence on near-surface atmospheric humidity, vertical vapor transport, and the thermal dynamics of the soil–atmosphere boundary layer (Anthony T & Marc B, 1998; Zhang et al., 2016). Saito et al. (2006) employed a modified HYDRUS-1D model to simultaneously simulate coupled liquid water, water vapor, and heat transport, revealing that near-surface vapor fluxes are highly sensitive to atmospheric conditions, particularly temperature-driven gradients. Goss & Madliger (2007) employed capacitive humidity sensors to show that vapor transport was largely confined to the upper few centimeters of soil, with the evaporation front remaining shallower than 3 cm even after three months of continuous drying. Similarly, Kohfahl et al. (2021) monitored vapor fluxes within a 1.5 m soil profile using high-precision weighing lysimeters and identified net radiation and vapor pressure deficit as the primary drivers of evaporation. While previous studies have characterized vapor dynamics in shallow soils, the fine-scale exchange processes near the soil–atmosphere interface—particularly the vertical coupling between the DSL and the overlying molecular diffusion layer—remain insufficiently understood. This knowledge gap is largely due to the lack of long-term, fine-scale in-situ observations, which limits our ability to clarify the vapor flux dynamics and their responses to meteorological forcing (van de Griend and Owe, 1994).

https://doi.org/10.5194/egusphere-2026-1143
Preprint. Discussion started: 6 March 2026


Fiber Bragg Grating (FBG) sensing is an emerging fiber-optic technology that offers several advantages, including compact size, high sensitivity, low power consumption, thermal stability, corrosion resistance, and the capability for long-distance wireless monitoring (Caucheteur et al., 2016; Mahmoud Aghdami et al., 2021; Zhang & Yao, 2018). In our previous study, miniaturized fiber Bragg grating (FBG)-based relative humidity sensors were deployed under controlled laboratory conditions to investigate vapor transport behavior in dry sand during evaporation (Guo et al., 2025). While that work provided valuable insights into subsurface vapor flux dynamics, it did not capture the fine-scale, in-situ vapor exchange processes occurring across the soil–atmosphere interface under natural environmental forcing. To address this gap, the present study conducted field experiments in a representative semi-arid area on the Chinese Loess Plateau (Baota District, Yan'an City, Shaanxi Province), where FBG sensors were embedded across the soil–atmosphere interface. This configuration enabled long-term, high-resolution monitoring of vertical vapor fluxes between the underlying DSL and the overlying molecular diffusion layer. Through this setup, we aimed to capture the temporal variability of near-surface vapor exchange and elucidate the meteorological control mechanisms that govern interfacial transport under dynamic climatic conditions.

## 2 Field monitoring and analytical methods

### 2.1 Site description

The experimental site is situated on the Loess Plateau in Baota District, Yan'an City, Shaanxi Province, China (36.46°N, 109.48°E), at an elevation of approximately 1155 m. This region lies within the transitional zone between arid and semi-arid climates and is characterized by a warm temperate continental monsoon climate (Zhao et al., 2019). The geographic location of the site is shown in Figure S1 in the Supporting Information. The long-term mean annual temperature is 9.8 °C, with monthly extremes ranging from –25.4 °C in January to 39.7 °C in July. The mean annual precipitation is 541 mm, of which 50%–70% occurs during the summer monsoon season (June–August). In contrast, the mean annual potential evaporation exceeds 1000 mm, indicating a persistent moisture deficit and a characteristic semi-arid hydrological regime. The local stratigraphy is dominated by Quaternary loess deposits (Sun et al., 2021). According to the Unified Soil Classification System (USCS), it is classified as low-plasticity silt (ML). Key physical properties of the native loess, including grain-size distribution and Atterberg limits, are summarized in Table S1 in the Supporting Information.

### 2.2 Field monitoring and setup

Various meteorological factors—including solar radiation, air temperature, relative humidity, wind speed, and precipitation—govern the coupled heat and moisture exchange between the soil and atmosphere (Figure 1a). To quantify vertical water vapor exchange across the soil–atmosphere interface, we employed a novel fiber-optic sensing technique using temperature and humidity sensors based on fiber Bragg grating (FBG) technology (Figure 1b). The sensing principles for both temperature and relative humidity measurements are described in Text S1 and illustrated in Figures S2 and S3 in the Supporting Information. The sensors were encapsulated within a breathable and waterproof probe to ensure mechanical durability and effective vapor

https://doi.org/10.5194/egusphere-2026-1143
Preprint. Discussion started: 6 March 2026


permeability while preventing liquid water intrusion (Guo et al., 2021, 2022). Previous evaluations have demonstrated that the sensors exhibit a compact form factor, high measurement accuracy, low hysteresis, excellent repeatability, and long-term stability (Guo et al., 2023). Key performance specifications are summarized in Table S3 in the Supporting Information.

The sensors were mounted on stainless steel brackets at predefined intervals and vertically embedded at three representative heights: 1 cm above the soil–atmosphere interface (Layer $_{air}$), directly at the interface, and 7 mm below it (Layer $_{soil}$). Three identical sets of FBG sensors were deployed to investigate spatial variations in vapor flux under different microclimatic conditions. Although this study focuses on bare soil surfaces, preliminary comparative data under vegetated and shaded conditions are provided in Figure S4 in the Supporting Information. In parallel, a compact automatic weather station was installed adjacent to the monitoring area to record meteorological variables—including solar radiation, wind speed, air temperature, relative humidity, and precipitation—at hourly intervals. The system was installed and commissioned in August 2022, with continuous field monitoring conducted from August 11, 2022, to June 30, 2023. A summary of the observed meteorological conditions during this period is presented in Figure S5 in the Supporting Information.

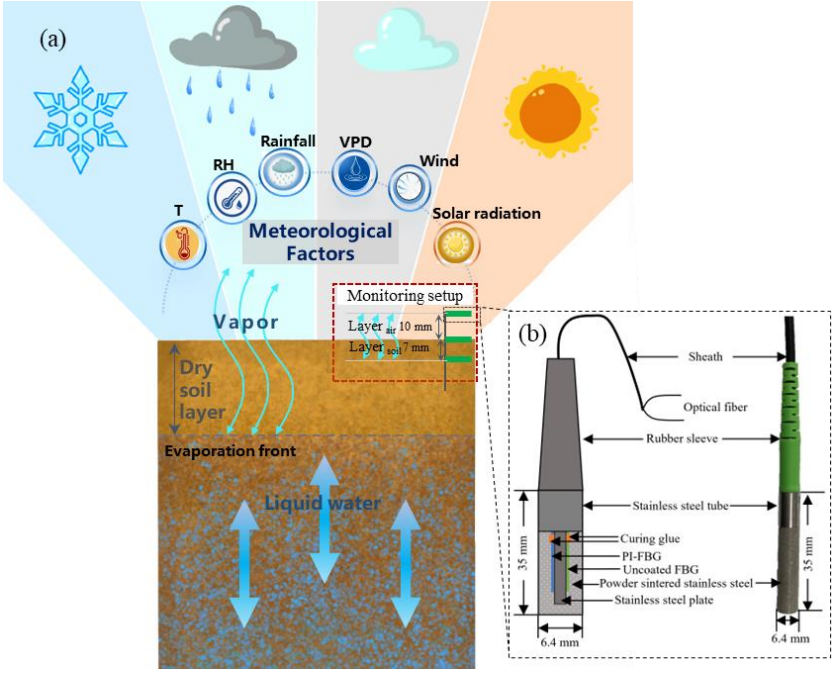


**Figure 1. Field monitoring setup and FBG sensor structure. (a) Schematic diagram of the sensor deployment configuration for vertical vapor flux monitoring at the soil–atmosphere interface. (b) Structural illustration of the PI-coated FBG temperature and humidity sensor used in this study. Technical specifications are listed in Table S2.**

### 2.3 Vertical water vapor flux calculation

Vertical water vapor flux refers to the amount of water vapor transported through a vertical cross-section per unit time (RASMUSSON, 1968). It characterizes both the direction and magnitude of vapor movement in the vertical dimension, with

https://doi.org/10.5194/egusphere-2026-1143
Preprint. Discussion started: 6 March 2026


positive values indicating upward transport (evaporation) and negative values representing downward transport (condensation). Based on the authors' previous research, vertical vapor flux between adjacent depths in unsaturated soils can be approximated using measurements from FBG-based relative humidity sensors, with detailed calculation procedures provided in Text S2 in the Supporting Information. The core formulation is as follows, adapted from Goss & Madliger (2007) and Penman (1940):

$$q_v = \Theta_a \tau \frac{D_1 \rho_{v1} - D_2 \rho_{v2}}{x_1 - x_2} \quad (1)$$

where $D_1$ and $D_2$ represent the diffusion coefficients of water vapor in air ($m^2\ d^{-1}$) at the temperatures corresponding to depths $x_1$ and $x_2$, respectively. Similarly, $\rho v_1$ and $\rho v_2$ denote the water vapor densities ($g\ m^{-3}$) at depths $x_1$ and $x_2$. The influence of thermal diffusion is considered negligible and thus is not included in the calculation.

In the near-surface region, particularly at small spatial scales, molecular diffusion dominates water vapor transport (Fetzer et al., 2017). The vertical vapor flux can be theoretically approximated by Fick's first law of diffusion:

$$q_v = -D_v \nabla \rho_v \quad (2)$$

where $D_v$ is the effective molecular diffusion coefficient for water vapor in air ($m^2\ s{-}1$). The dependence of the diffusion coefficient $D_v$ on temperature T can be estimated using the following empirical relation (Massman, 1998):

$$D = D_0 \left(\frac{T}{T_0}\right)^n \quad (3)$$

where $D_0$ is the diffusion coefficient at the reference temperature $T_0$, typically taken as $2.5\times10^{-5}$ $m^2/s$ at 25°C (298 K), T is the target air temperature in Kelvin (K), n is an empirical exponent, usually around 1.5, although it may vary slightly depending on experimental conditions, $T_0$ is the reference temperature, commonly 298 K.

### 2.4 Statistical Analysis

Structural Equation Modeling (SEM) is a multivariate statistical technique that integrates path analysis with latent variable modeling, enabling simultaneous estimation of multiple causal pathways and quantification of both direct and indirect relationships among variables (Li et al., 2024). Compared to conventional regression models, SEM is particularly well-suited for revealing hierarchical structures and coupled mechanisms in complex systems, thereby facilitating comprehensive interpretation and mechanism-oriented exploration of multidimensional data. To investigate the influence of meteorological factors on vapor fluxes across the soil–atmosphere interface, vapor flux data recorded at 10-minute intervals were first aggregated to an hourly timescale to align with corresponding meteorological observations. Based on 5,657 valid data points obtained from field monitoring, SEM was employed to examine the direct and indirect effects of solar radiation, precipitation, time since last rainfall, air temperature, and relative humidity on near-surface vapor fluxes (i.e., within both Layer $_{air}$ and Layer $_{soil}$). Model development began with a priori specification of all hypothesized pathways, followed by stepwise elimination of

https://doi.org/10.5194/egusphere-2026-1143
Preprint. Discussion started: 6 March 2026


non-significant paths to achieve a parsimonious final model. Model fit was evaluated using Fisher's C statistic as implemented in the "piecewiseSEM" package within the R 4.2.2 environment.

## 3 Dynamic variation of vapor fluxes under clear-sky conditions

### 3.1 Diurnal response of vapor fluxes to solar radiation

From October 22 to 25, 2022, a continuous three-day clear-sky period was selected to investigate the diurnal dynamics of vapor fluxes. Solar radiation (Figure 2a) exhibited a typical unimodal diurnal pattern, peaking near midday. With increasing radiation, air temperature (Figure 2b) rose steadily, while relative humidity (Figure 2c) declined inversely. Vertically, relative humidity remained higher and more stable near the soil surface, whereas values at greater heights were lower and more variable, closely reflecting ambient atmospheric conditions. This stratification arises from the enclosed and near-saturated humidity environment within soil pores, in contrast to the interface zone, which is jointly influenced by subsurface moisture and atmospheric fluctuations. Consequently, a distinct vertical humidity gradient is established across the interface.

Solar radiation absorbed at the surface is converted into heat, creating pronounced gradients in both temperature and humidity across the soil–atmosphere transition. As radiation intensifies during the day, the vapor pressure deficit (VPD)—the difference between saturated and actual vapor pressure (Figure 2d)—also increases, indicating drier air and enhanced atmospheric demand for moisture. This strengthens the humidity gradient and promotes upward vapor transport, leading to a marked increase in vapor flux across the interface (Figure 2e).

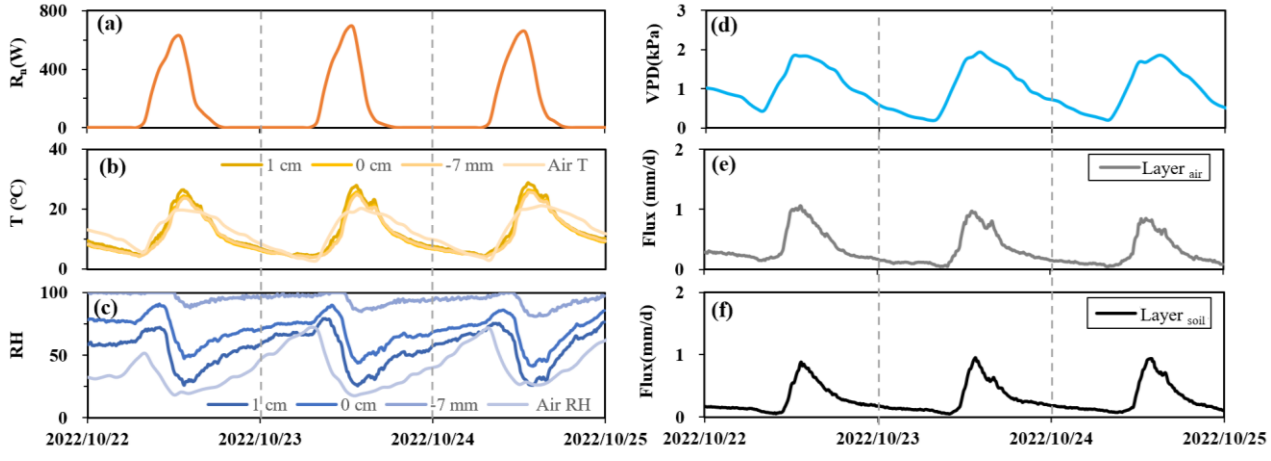


**Figure 2. Diurnal evolution of key variables under clear-sky conditions from October 22 to 25, 2022: (a) solar radiation (Rn); (b) air temperature (T); (c) relative humidity (RH) at multiple heights across the soil–atmosphere interface; (d) vapor pressure deficit (VPD); (e) vertical water vapor flux of Layer air; (f) vertical water vapor flux of Layer soil. All variables exhibit pronounced diurnal cycles, with vapor flux patterns reflecting the combined influence of radiative forcing, thermal gradients, and humidity stratification.**

https://doi.org/10.5194/egusphere-2026-1143
Preprint. Discussion started: 6 March 2026


Overall, under clear-sky conditions, solar radiation constitutes the dominant external forcing. The concomitant increase in air temperature and decrease in relative humidity elevate the vapor pressure deficit (VPD), thereby intensifying evaporative demand and promoting soil water loss to the atmosphere. These tightly coupled processes collectively drive pronounced diurnal variations in solar radiation, VPD, relative humidity, and vapor flux across the soil–atmosphere interface.

### 3.2 Diurnal response of vapor flux to solar radiation across different seasons

The fiber-optic sensors employed in this study successfully captured seasonal variations in vapor flux dynamics near the soil–atmosphere interface. Representative clear-sky days from each season were selected to examine the diurnal response of vapor fluxes in the Layer $_{soil}$ and Layer $_{air}$ zones to solar radiation. Results revealed distinct diurnal patterns and time-lagged responses, with flux intensity and lag duration varying markedly by season.

In autumn (Figure 3a) and spring (Figure 3c), vapor fluxes in the Layer $_{soil}$ exhibited pronounced diurnal cycles, rising from approximately 0.2 mm $d^{-1}$ in the early morning to peak values later in the day. Peak fluxes generally lagged solar radiation by around 30 minutes, while the initial increase was delayed by 2–3 hours. This lagged response reflects the time required to establish vertical gradients in temperature and humidity, compounded by the soil's high specific heat capacity, which retards thermal equilibration. After sunset, residual heat conduction from daytime energy storage sustained vapor diffusion, resulting in a gradual decline in vapor fluxes. Vapor fluxes in the Layer $_{air}$ exhibited a similar diurnal pattern but responded more promptly to radiative forcing due to the lower thermal mass of the overlying air column.

In winter (Figure 3b), vapor fluxes were substantially reduced due to weak solar forcing and low ambient temperatures. Peak fluxes in the Layer $_{air}$ reached only ~0.13 mm $d^{-1}$, while those in the Layer $_{soil}$ exhibited the most pronounced seasonal lag—initiating approximately 3.5 hours after sunrise and peaking around 2.5 hours after the solar radiation maximum. This delayed response reflects the limited availability of radiative energy and the presence of frozen soil moisture, which constrains thermal transfer. The high specific heat and low thermal conductivity of ice, combined with latent heat effects associated with phase transitions, further retard heat propagation. Additionally, the formation of a frozen layer inhibits nocturnal vapor migration, resulting in both suppressed magnitudes and prolonged response times in near-surface vapor fluxes.

In contrast, summer conditions (Figure 3d) exhibited the highest vapor flux magnitudes, with peak values approaching 1.0 mm $d^{-1}$ in the Layer soil and 1.4 mm $d^{-1}$ in the Layer air. Vapor fluxes responded acutely to short-term fluctuations in solar radiation, demonstrating a high degree of radiative sensitivity under elevated temperature conditions. Although the onset of flux increase lagged solar radiation by approximately 4 hours, peak fluxes occurred rapidly thereafter. Notably, a transient reduction in irradiance around 13:00 induced an immediate decline in vapor fluxes, underscoring the strong coupling between radiative forcing and vapor exchange processes during the warm season. A detailed quantitative analysis of seasonal lag characteristics is provided in the subsequent section.

https://doi.org/10.5194/egusphere-2026-1143
Preprint. Discussion started: 6 March 2026


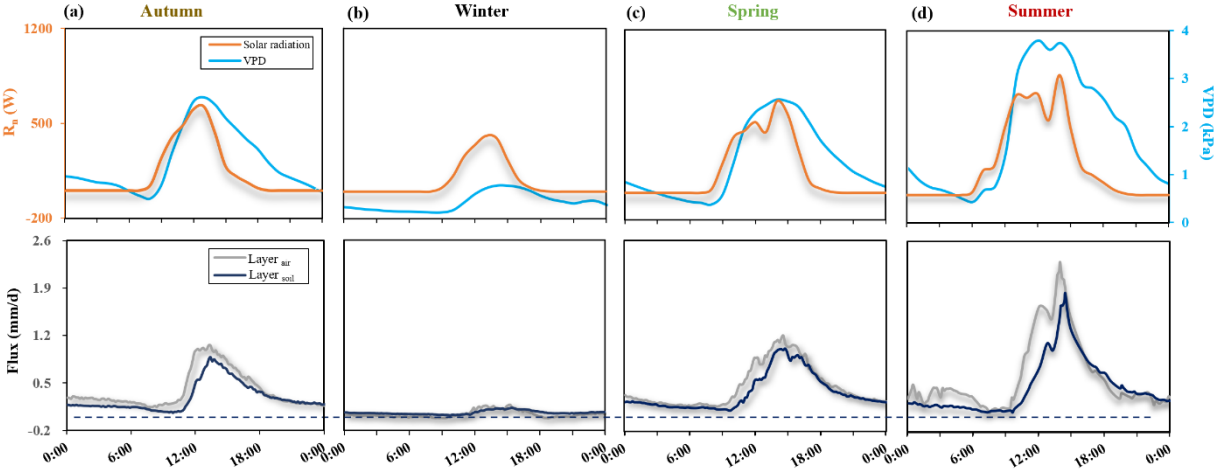


**Figure 3. Diurnal variations of vertical vapor fluxes under representative clear-sky conditions in different seasons: (a) autumn (22 October 2022), (b) winter (5 January 2023), (c) spring (6 March 2023), and (d) summer (24 June 2023). The upper row shows solar radiation and VPD, and the lower row presents the corresponding vertical vapor fluxes near the soil–atmosphere interface.**

### 3.3 Lag characteristics of vapor fluxes in response to solar radiation

Vapor fluxes in the Layer $_{soil}$ (below the interface) responded to solar radiation with a greater delay than those in the Layer $_{air}$ (above the interface), indicating an asynchronous and depth-dependent response to radiative forcing. This reflects a stepwise transfer of energy and vapor-driving gradients, initiated by surface energy changes and subsequently propagated downward. To characterize this dynamic coupling, a time-lag-adjusted cross-correlation analysis was applied to examine the relationship between solar radiation and daytime vapor fluxes. After correcting for lag, strong linear correlations were observed across all seasons. Due to differences in temporal resolution between radiation (hourly) and flux data (10-minute), this section emphasizes the relative lag between the two layers rather than absolute lag quantification.

In autumn (Figure 4a) and spring (Figure 4c), moderate solar radiation and relatively efficient heat and moisture transfer in the near-surface soil led to a lag of approximately 30 minutes in Layer $_{soil}$ vapor fluxes compared to those in Layer $_{air}$. In winter (Figure 4b), weakened radiative input significantly slowed soil warming and vapor diffusion, resulting in an extended lag of up to 120 minutes. Despite the limited solar forcing, time-lag-corrected analysis revealed strong linear correlations between vapor flux and radiation, indicating that coupled heat–mass transfer processes remained active, albeit with reduced responsiveness. In summer (Figure 4d), intense solar radiation and more heterogeneous surface moisture and energy conditions introduced complexity to the vapor transport dynamics. This yielded an intermediate lag of around 60 minutes, reflecting the combined effects of strong radiative forcing and vertical heterogeneity in soil structure, moisture distribution, and thermal diffusivity. These factors collectively attenuated the direct transmission of energy and vapor-driving gradients to deeper soil layers, thereby limiting the immediacy of the Layer $_{soil}$ response.

https://doi.org/10.5194/egusphere-2026-1143
Preprint. Discussion started: 6 March 2026


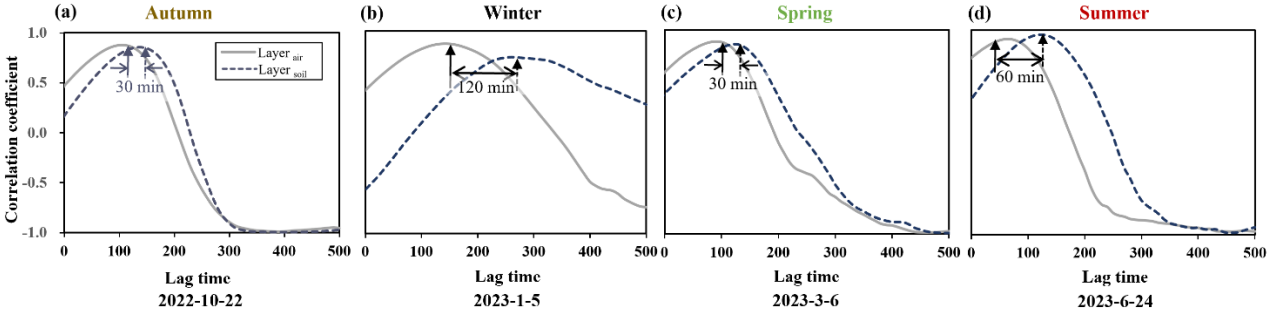


**Figure 4. Lagged response of vapor fluxes in Layer soil and Layer air to solar radiation: (a) Autumn (2022-10-22), lag = 30 min; (b) Winter (2023-01-05), lag = 120 min; (c) Spring (2023-03-06), lag = 30 min; (d) Summer (2023-06-24), lag = 60 min.**

## 4 Dynamic behavior of vapor fluxes under rainfall conditions

### 4.1 Immediate response of vapor fluxes to rainfall

Taking the rainfall event on June 18, 2023, as a representative case, solar radiation dropped sharply during precipitation due to dense cloud cover (Figure 5a), resulting in insufficient energy input to sustain evaporation. Concurrently, atmospheric humidity approached saturation, and the VPD declined to near zero (Figure 5b), effectively eliminating the vapor transport potential. Rainwater infiltration elevated shallow soil moisture, driving relative humidity near the soil–atmosphere interface to 100% RH (Figure 5c). Under these near-saturated conditions, VPD remained minimal and vapor fluxes were nearly suppressed (Figure 5d). After rainfall ceased, solar radiation recovered rapidly, and VPD increased with a slight lag due to a gradual decrease in atmospheric humidity. However, the interface zone remained near saturation due to high residual soil moisture, resulting in only a delayed and weak decline in RH. It was not until the third day that solar heating re-established a meaningful humidity gradient near the interface, enabling vapor fluxes—particularly in the Layer air—to resume.

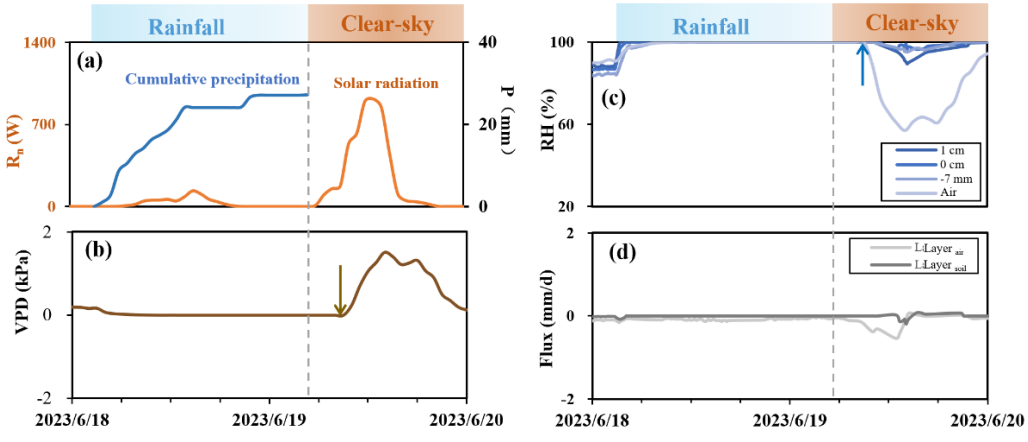


**Figure 5. Variations in key parameters during and after the rainfall event on June 18, 2023: (a) Rn and P (Cumulative precipitation); (b) VPD; (c) RH; and (d) Flux.**

https://doi.org/10.5194/egusphere-2026-1143
Preprint. Discussion started: 6 March 2026


### 4.2 Post-rainfall response of vapor fluxes

Using the rainfall event on June 18, 2023, as a representative case, the subsequent clear-sky period was characterized by a rapid rebound in solar radiation (Figure 6a), which reestablished the energy input necessary to sustain soil evaporation and vapor transport. Near the soil–atmosphere interface, relative humidity exhibited a pronounced diurnal pattern (Figure 6b), with daytime minima progressively decreasing over successive days. This trend indicates enhanced surface drying and increased sensitivity to atmospheric forcing. In the shallow 7 mm soil layer, RH remained near saturation during the initial post-rain days, suggesting the presence of liquid water. With continued solar input, RH minima declined and diurnal amplitudes intensified, reflecting the downward migration of the evaporation front as surface moisture was gradually depleted. Simultaneously, VPD rose sharply under clear-sky conditions, significantly strengthening the vapor pressure gradient and promoting upward vapor fluxes (Figure 6c). A stratified response emerged, wherein vapor fluxes in the Layer $_{air}$ recovered quickly and stabilized due to sustained surface moisture availability, while those within the Layer $_{soil}$ increased more gradually. This delayed enhancement highlights the progressive intensification of internal soil evaporation as the drying front advanced downward over time.

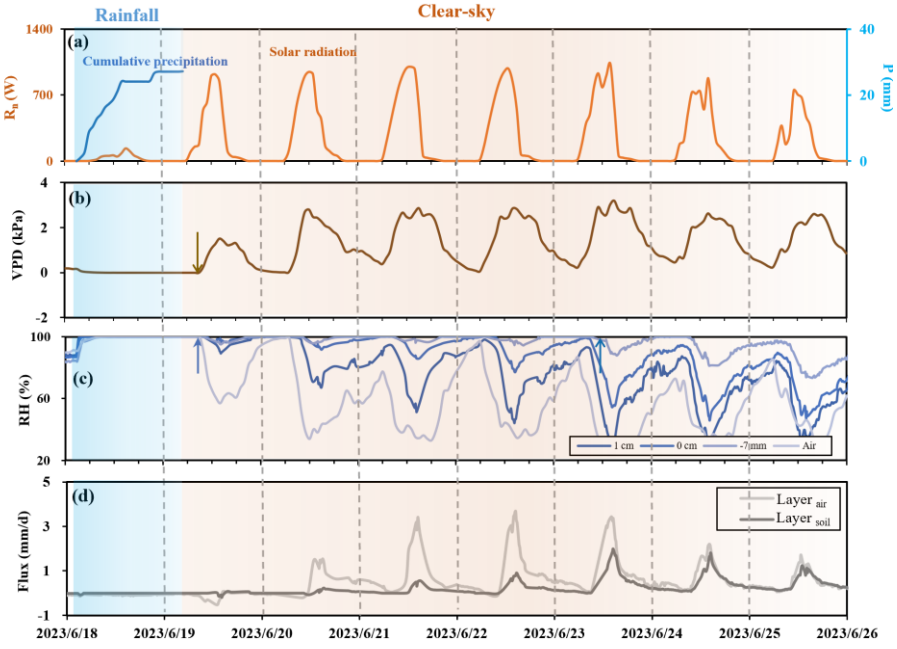


**Figure 6. Variations in key parameters during and after the rainfall event on June 18, 2023: (a) Rn; (b) RH; (c) Flux.**

### 4.3 Seasonal response characteristics of vapor fluxes to rainfall

This section investigates the seasonal variability in vapor flux responses near the soil–atmosphere interface under rainfall conditions and during subsequent clear-sky periods. In autumn (Figure 7a), characterized by declining solar radiation and frequent light-to-moderate precipitation, the rainfall event on October 13 occurred in the early morning. Due to the persistently low incoming radiation that followed, vapor fluxes in both the Layer $_{air}$ and Layer $_{soil}$ remained near zero. As solar radiation

https://doi.org/10.5194/egusphere-2026-1143
Preprint. Discussion started: 6 March 2026


gradually recovered, vapor fluxes in the Layer $_{air}$ responded rapidly, whereas those in the Layer soil increased more gradually, reflecting differences in thermal inertia and moisture redistribution between the two layers. In spring (Figure 7c), rainfall was typically light and short in duration, coinciding with moderate solar radiation. On March 23, a brief overnight rainfall followed by rapid clearing triggered a marked increase in vapor fluxes in both layers, including a swift response in the Layer $_{soil}$. This indicates that even minor precipitation events can substantially alter shallow soil moisture, thereby enhancing vapor fluxes below the interface, while fluxes above the interface remain predominantly controlled by solar radiation. In winter (Figure 7b), low temperatures, reduced radiation, and precipitation primarily in the form of snow collectively suppressed soil evaporation, resulting in the lowest vapor flux magnitudes observed throughout the year. Snow cover further impeded vapor exchange by thermally and physically decoupling the soil from the atmosphere. Even during snowmelt episodes, only limited and short-lived increases in vapor flux were observed, with overall exchange rates remaining minimal. By contrast, summer (Figure 7d) was marked by the combined effects of high-intensity precipitation and strong solar radiation. During the prolonged and intense rainfall event on June 18–19, vapor fluxes in the Layer $_{air}$ remained near zero despite elevated post-rain radiation levels, suggesting that the large influx of water saturated the surface soil and temporarily inhibited vapor exchange with the atmosphere. In the Layer $_{soil}$, vapor fluxes increased more slowly but consistently as evaporation resumed under rising solar input. This stratified and lagged recovery pattern underscores the critical role of antecedent soil moisture and radiative forcing in governing vapor transport dynamics near the soil–atmosphere interface.

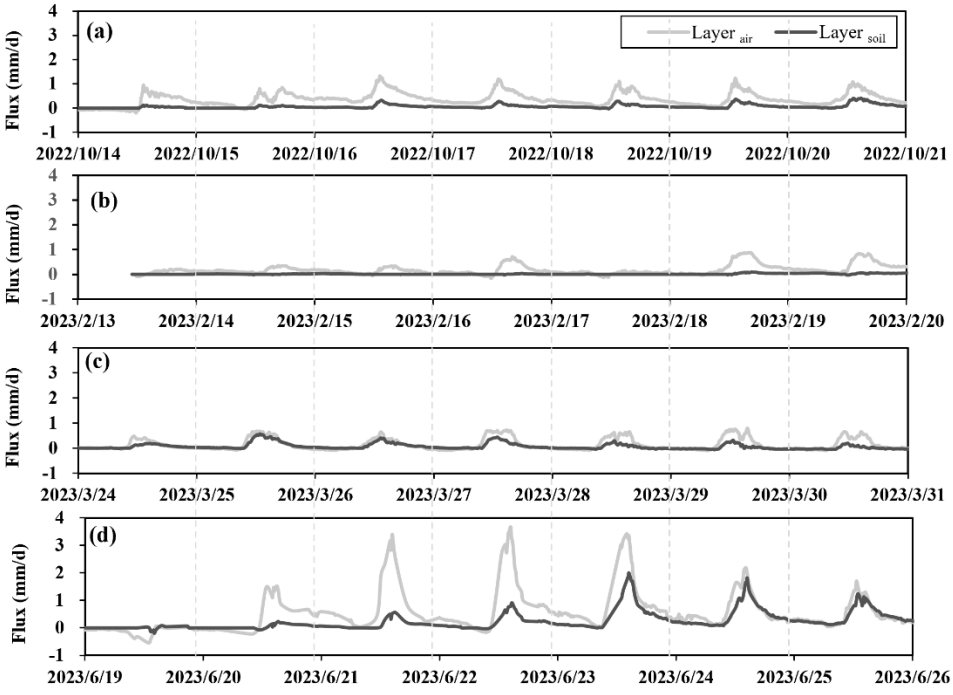


**Figure 7. Seasonal variations in vapor flux dynamics during and after precipitation events: (a) Autumn (October 14–21, 2022), with a cumulative rainfall of 1.4 mm and daily peak solar radiation ranging from 476 to 758.1 W m$^{-2}$; (b) Winter (February 13–20, 2023),**

https://doi.org/10.5194/egusphere-2026-1143
Preprint. Discussion started: 6 March 2026


**with a cumulative snowfall equivalent of 6.7 mm and daily peak solar radiation ranging from 42.66 to 612.8 W m$^{-2}$; (c) Spring (March 24–31, 2023), with a cumulative rainfall of 0.4 mm and daily peak solar radiation ranging from 347.6 to 824 W m$^{-2}$; (d) Summer (June 19–26, 2023), with a cumulative rainfall of 27.2 mm and daily peak solar radiation ranging from 747.3 to 1028 W m$^{-2}$.**

## 5 Influence of Meteorological Factors on Vapor Flux Across the Soil–Atmosphere Interface

Using a monitoring dataset of 5657 valid observations, we applied Structural Equation Modeling (SEM) to analyze the direct and indirect effects of key meteorological factors—solar radiation, precipitation, time since last rainfall, air temperature, and relative humidity—on near-surface vapor fluxes in both the Layer $_{air}$ and Layer soil.

### 5.1 Structural Equation Modeling of Vapor Flux in Layer $_{air}$

As illustrated in Figure 8, the SEM results reveal that multiple meteorological factors influence Flux Layer air through diverse pathways. Solar radiation, precipitation, and relative humidity primarily exert indirect effects by modulating intermediate variables such as air temperature, humidity, and particularly vapor pressure deficit (VPD). In contrast, time since last rainfall and air temperature exhibit modest but direct negative effects. These findings highlight the sensitivity of Flux Layer air in semi-arid environments, where soil moisture acts as a limiting factor, to short-term hydrometeorological fluctuations and surface moisture availability. Specifically, prolonged time since last rainfall leads to rapid soil moisture depletion. While evaporative potential may increase, the actual vapor flux is constrained by limited liquid water availability, resulting in a slight reduction in Flux Layer air. Similarly, although higher air temperatures theoretically enhance evaporation, their primary positive influence is already mediated through VPD. The residual direct negative effect of air temperature in the SEM may reflect the interplay between atmospheric drying and accelerated soil moisture loss under high temperatures, exacerbating moisture limitations.

Notably, VPD demonstrates the strongest and statistically significant direct positive effect on Flux Layer air (path coefficient: 0.62***), establishing it as the dominant driver of vapor flux in this layer. Collectively, the SEM delineates a coordinated regulatory system where multiple factors interact—both directly and indirectly—to govern vapor transport, with VPD serving as the central dynamic mechanism.

https://doi.org/10.5194/egusphere-2026-1143
Preprint. Discussion started: 6 March 2026


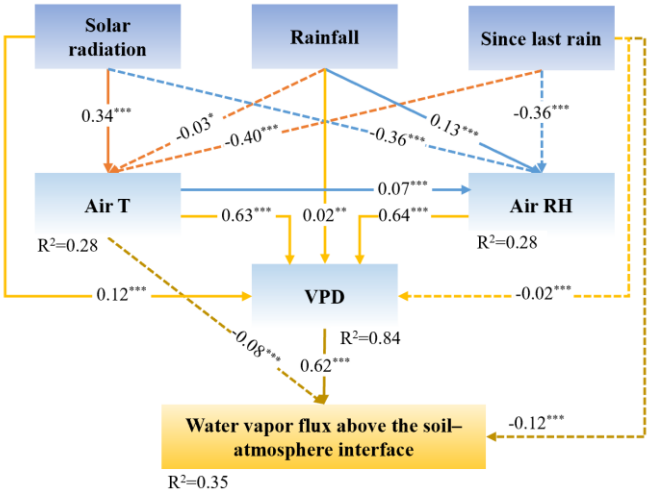


**Figure 8. Structural equation model (SEM) illustrating the direct and indirect effects of meteorological factors on near-surface vapor flux in the above-interface air layer (Layer $_{air}$).**

The model evaluates the effects of solar radiation, air temperature, relative humidity, precipitation, and time since last rainfall on vapor flux in Layer_air (Fisher's C = 9.695; P = 0.138; df = 6; n = 5657 observations). Solid arrows indicate significant positive effects, while dashed arrows indicate significant negative effects. Arrow colors represent different response variables; arrows of the same color point to the same variable. Numbers adjacent to arrows denote standardized path coefficients. $R^2$ indicates the proportion of variance explained. Significance levels: P < 0.05 (*), P < 0.01 (**), P < 0.001 (***).

## 5.2 Structural equation modelling of vapor flux in Layer $_{soil}$

As with Layer $_{air}$, the VPD emerges as the primary driver of Flux Layer $_{soil}$, exhibiting the strongest standardized path coefficient (0.79***), slightly higher than that for Layer air (0.62***). This elevated sensitivity underscores the critical role of VPD in governing vapor transport within unsaturated soils, where internal vapor migration is predominantly driven by vapor pressure gradients. In such conditions, the movement of water vapor from soil pores to the atmosphere requires overcoming diffusive resistance, making a sustained VPD essential for maintaining upward flux. The time since the last rainfall exerts a positive direct effect on Flux Layer $_{soil}$, in contrast to its negative effect on Flux Layer $_{air}$, reflecting a clear divergence in post-precipitation regulatory mechanisms between the two layers. As the interval following rainfall increases, surface soils progressively dry, the evaporation front migrates downward, and subsurface vapor transport intensifies, leading to an increase in Flux Layer $_{soil}$. In comparison, Flux Layer $_{air}$ may initially exhibit elevated fluxes due to near-surface moisture, but these fluxes typically diminish as surface drying advances and limits evaporative exchange. Moreover, Flux Layer $_{soil}$ is subject to additional but weaker direct influences from solar radiation and atmospheric humidity. Solar radiation shows a slight negative effect (–0.10***), while atmospheric humidity has a modest positive effect (0.07***). The negative radiative influence likely reflects residual suppression effects, wherein intense radiation accelerates surface drying and attenuates vapor gradients,

https://doi.org/10.5194/egusphere-2026-1143
Preprint. Discussion started: 6 March 2026


thereby transiently inhibiting deeper vapor flux. Conversely, higher atmospheric humidity may help maintain near-surface moisture conditions, indirectly slowing moisture depletion and sustaining vapor diffusion.

Collectively, while VPD remains the dominant mediator through indirect pathways, these minor direct effects illustrate the subtle but important role of microclimatic conditions in regulating subsurface vapor fluxes in unsaturated soils.

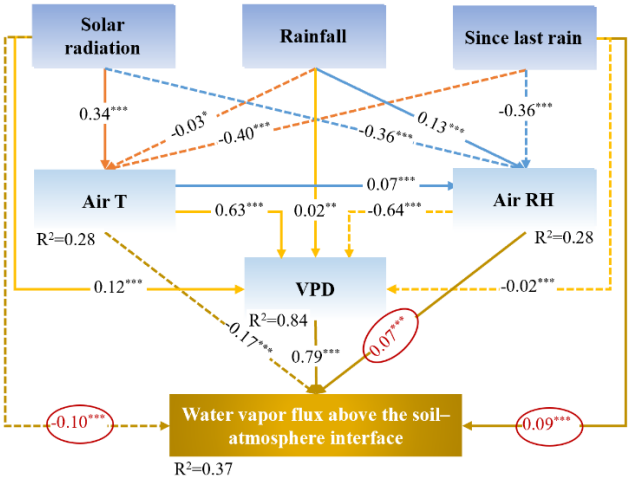


**Figure 9. Structural equation model (SEM) illustrating the direct and indirect effects of meteorological factors on near-surface vapor flux in the subsurface soil layer (Layer soil). Model structure, arrow notation, and significance level indicators are consistent with Figure 8. (Fisher's C = 2.339; P = 0.31; df = 2; n = 5657 observations.) Red elements in the figure highlight differences from the structure shown in Figure 8.**

## 6 Conclusions

This study presents a comprehensive investigation of soil-atmosphere vapor exchange dynamics in a semi-arid loess region using advanced fiber Bragg grating (FBG) sensing technology. Through nearly one year of continuous high-resolution monitoring, we have successfully characterized the fine-scale water vapor transport processes occurring across the soil-atmosphere interface, with particular focus on the 7 mm subsurface soil layer (Layer $_{soil}$) and the 10 mm atmospheric boundary layer (Layer $_{air}$). Our approach effectively addresses the resolution limitations of conventional eddy covariance methods in capturing molecular-scale transport phenomena. The principal findings can be summarized as follows:

(1) Under typical clear-sky conditions, vertical vapor fluxes across the soil–atmosphere interface exhibit pronounced diurnal variability, primarily governed by solar radiation and further modulated by air temperature, relative humidity, and vapor pressure deficit (VPD). Observational data reveal a distinct lag in the response of vapor flux to solar forcing, with Layer $_{air}$ showing a more rapid adjustment, while Layer $_{soil}$ exhibits a delayed response due to constraints associated with thermal conduction and the temporal development of diffusion gradients. Seasonally, vapor fluxes are moderate with intermediate lags

https://doi.org/10.5194/egusphere-2026-1143
Preprint. Discussion started: 6 March 2026


in spring and autumn, minimal and most delayed in winter, and highest with the greatest diurnal amplitude in summer—reflecting a stratified seasonal response regime.

(2) During rainfall events and the ensuing recovery under clear-sky conditions, the vertical profiles of vapor flux demonstrate marked asymmetry in space and time. Precipitation suppresses vapor exchange by reducing solar radiation and elevating ambient humidity, leading to a near-zero VPD and thus the cessation of evaporation. Following rainfall cessation, Layer $_{air}$ flux rapidly increases in response to recovering solar input and VPD, whereas Layer $_{soil}$ flux responds more gradually, reflecting the delayed onset of surface drying, downward migration of the evaporation front, and the establishment of strengthened vapor gradients. Notably, these dynamics are modulated by seasonal context: in winter, flux responses are weak due to low temperatures and snow cover; in spring and autumn, variations are minor; in summer, vapor flux increases sharply after a delayed onset, driven by the coupled effects of intense rainfall and high radiation.

(3) Structural equation modeling (SEM) was employed to elucidate the direct and indirect causal pathways through which meteorological variables influence near-surface vapor flux. The analysis identifies VPD as the dominant proximal driver, exerting statistically significant positive effects on vapor flux in both Layer $_{air}$ (standardized path coefficient = 0.62***) and Layer $_{soil}$ (0.79***). Time since last rainfall exerts a minor negative effect on Layer $_{air}$ but a positive effect on Layer $_{soil}$, indicating that progressive drying reduces vapor release from the surface layer while enhancing internal vapor diffusion from the subsurface. These findings suggest a stratified flux regime controlled by the dynamic downward displacement of the evaporation front under drying conditions.

These findings advance the mechanistic understanding of soil–atmosphere coupling and underscore the utility of FBG-based sensing for capturing fine-scale vapor transport in drylands. From a surface hydrology perspective, the work provides crucial observational constraints on near-surface evaporation processes, improves the representation of vapor-phase fluxes in hydrological models, and informs drought-resilient water balance assessments under future climate conditions.

**Code, data, or code and data availability**

The fiber-optic sensing dataset used to quantify water vapor flux across the soil–atmosphere interface is available on Zenodo at https://doi.org/10.5281/zenodo.15857069. Meteorological data from the on-site weather station collected during the monitoring period are archived in the same repository at https://doi.org/10.5281/zenodo.15857109. The R code used for structural equation modeling (SEM) and data analysis is available at https://doi.org/10.5281/zenodo.15857131.

https://doi.org/10.5194/egusphere-2026-1143
Preprint. Discussion started: 6 March 2026


## Author contributions

Junyi Guo: Conceptualization, Data curation, Formal analysis, Writing – original draft. Mengya Sun: Data curation, Project administration. Chengcheng Zhang: Visualization, Writing – review & editing. Jie Liu: Resources, Validation. Qingnan Lou: Investigation, Resources. Qiyu Xu: Investigation, Resources. Bin Shi: Supervision, Resources, Project administration, Funding acquisition.

## Competing interests

The authors declare that they have no conflict of interest.

## Acknowledgements

The authors warmly thank Guangqing Wei, Lixiang Jia, Junwei Lu, and Jinfeng Zhang from Suzhou Nanzee Sensing Technology Co., Ltd for their technical assistance.

## Financial support

This research was financially supported by the National Natural Science Foundation of China, NSFC (Grant Nos. 423B2704, 42030701, 42307189).

## References

Anthony T, C. and Marc B, P.: On water vapor transport in field soils, Water Resources Research, 34, 731–739, 1998.

Bagley, J. E., Kueppers, L. M., Billesbach, D. P., Williams, I. N., Biraud, S. C., and Torn, M. S.: The influence of land cover on surface energy partitioning and evaporative fraction regimes in the U.S. Southern Great Plains, Journal of Geophysical Research, 122, 5793–5807, https://doi.org/10.1002/2017JD026740, 2017.

Caucheteur, C., Guo, T., Liu, F., Guan, B. O., and Albert, J.: Ultrasensitive plasmonic sensing in air using optical fibre spectral combs, Nature Communications, 7, 1–8, https://doi.org/10.1038/ncomms13371, 2016.

Chatterjee, D., Nayak, A. K., Vijayakumar, S., Debnath, M., Chatterjee, S., Swain, C. K., Bihari, P., Mohanty, S., Tripathi, R., Shahid, M., Kumar, A., and Pathak, H.: Water vapor flux in tropical lowland rice, Environmental Monitoring and Assessment, 191, https://doi.org/10.1007/s10661-019-7709-4, 2019.

Choi, T., Hong, J., Kim, J., Lee, H., Asanuma, J., Ishikawa, H., Tsukamoto, O., Zhiqui, G., Ma, Y., Ueno, K., Wang, J., Koike, T., and Yasunari, T.: Turbulent exchange of heat, water vapor, and momentum over a Tibetan prairie by eddy covariance and

https://doi.org/10.5194/egusphere-2026-1143
Preprint. Discussion started: 6 March 2026


flux variance measurements, Journal of Geophysical Research D: Atmospheres, 109, 1–12, https://doi.org/10.1029/2004JD004767, 2004.

Du, C., Yu, J., Wang, P., and Zhang, Y.: Analysing the mechanisms of soil water and vapour transport in the desert vadose zone of the extremely arid region of northern China, Journal of Hydrology, 558, 592–606, https://doi.org/10.1016/j.jhydrol.2017.09.054, 2018.

Fetzer, T., Jan, V., Klaus, M., M.Smits, K., and Rainer, H.: Heat and water transport in soils and across the soil-atmosphere interface: 1. Theory and different model concepts, Water Resources Research, 53, 1057–1079, https://doi.org/10.1002/2016WR019983.Heat, 2017.

Goss, K. U. and Madliger, M.: Estimation of water transport based on in situ measurements of relative humidity and temperature in a dry Tanzanian soil, Water Resources Research, 43, 1–10, https://doi.org/10.1029/2006WR005197, 2007.

van de Griend, A. A. and Owe, M.: Bare soil surface resistance to evaporation by vapor diffusion under semiarid conditions, Water Resources Research, 30, 181–188, https://doi.org/10.1029/93WR02747, 1994.

Gu, L., Meyers, T., Pallardy, S. G., Hanson, P. J., Yang, B., Heuer, M., Hosman, K. P., Riggs, J. S., Sluss, D., and Wullschleger, S. D.: Direct and indirect effects of atmospheric conditions and soil moisture on surface energy partitioning revealed by a prolonged drought at a temperate forest site, Journal of Geophysical Research Atmospheres, 111, https://doi.org/10.1029/2006JD007161, 2006.

Guo, J., Sun, M., Zhang, C., Lienhart, W., Jiang, H., and Shi, B.: Water Vapor Transport in Dry Sand During Evaporation Monitored by Quasi-Distributed Fiber-Optic Sensing Technology, Water Resources Research, 61, https://doi.org/10.1029/2024WR038719, 2025.

Guo, J. Y., Shi, B., Sun, M. Y., Zhang, C. C., Wei, G. Q., and Liu, J.: Characterization of an ORMOCER®-coated FBG sensor for relative humidity sensing, Measurement: Journal of the International Measurement Confederation, 171, 108851, https://doi.org/10.1016/j.measurement.2020.108851, 2021.

Guo, J. Y., Shi, B., Sun, M. Y., Cheng, W., Zhang, C. C., Wei, G. Q., and Wang, X.: Application of PI-FBG sensor for humidity measurement in unsaturated soils, Measurement: Journal of the International Measurement Confederation, 188, 110415, https://doi.org/10.1016/j.measurement.2021.110415, 2022.

Guo, J. Y., Shi, B., Sun, M. Y., Zhang, C. C., Tang, C. S., Wei, G. Q., Fang, J. H., and Jiang, H. T.: Soil total suction sensing using fiber-optic technology, Geoderma, 439, 116687, https://doi.org/10.1016/j.geoderma.2023.116687, 2023.

Humphrey, V., Berg, A., Ciais, P., Gentine, P., Jung, M., Reichstein, M., Seneviratne, S. I., and Frankenberg, C.: Soil moisture–atmosphere feedback dominates land carbon uptake variability, Nature, 592, 65–69, https://doi.org/10.1038/s41586-021-03325-5, 2021.

Kohfahl, C., Saaltink, M. W., and Ruiz Bermudo, F.: Vapor flow control in dune sediments under dry bare soil conditions, Science of the Total Environment, 786, 147404, https://doi.org/10.1016/j.scitotenv.2021.147404, 2021.

https://doi.org/10.5194/egusphere-2026-1143
Preprint. Discussion started: 6 March 2026


Lehmann, P., Neuweiler, I., Vanderborght, J., and Vogel, H.-J.: Dynamics of Fluid Interfaces and Flow and Transport across Material Interfaces in Porous Media-Modeling and Observations, Vadose Zone Journal, 11, vzj2012.0105, https://doi.org/10.2136/vzj2012.0105, 2012.

Li, J., Pei, J., Fang, C., Li, B., and Nie, M.: Drought may exacerbate dryland soil inorganic carbon loss under warming climate conditions, Nature Communications, 15, 1–10, https://doi.org/10.1038/s41467-024-44895-y, 2024.

Liu, X., Zhan, W., Zhu, D., Wu, N., He, Y., and Chen, H.: Seasonal and interannual dynamics of water vapor flux at a fen in the Zoige peatlands on the Qinghai-Tibetan Plateau: four-year measurements, Journal of Hydrology, 612, https://doi.org/10.1016/j.jhydrol.2022.128058, 2022.

Mahmoud Aghdami, K., Rahnama, A., Ertorer, E., and Herman, P. R.: Laser nano-filament explosion for enabling open-grating sensing in optical fibre, Nature Communications, 12, https://doi.org/10.1038/s41467-021-26671-4, 2021.

Massman, W. J.: A review of the molecular diffusivities of H2O, CO2, CH4, CO, O3, SO2, NH3, N2O, NO, and NO2 in air, O2 and N2 near STP, Atmospheric Environment, 32, 1111–1127, https://doi.org/10.1016/S1352-2310(97)00391-9, 1998.

McHugh, T. A., Morrissey, E. M., Reed, S. C., Hungate, B. A., and Schwartz, E.: Water from air: An overlooked source of moisture in arid and semiarid regions, Scientific Reports, 5, 1–6, https://doi.org/10.1038/srep13767, 2015.

Meng, X., Wang, H., Wu, Y., Long, A., Wang, J., Shi, C., and Ji, X.: Investigating spatiotemporal changes of the land-surface processes in Xinjiang using high-resolution CLM3.5 and CLDAS: Soil temperature, Scientific Reports, 7, 1–14, https://doi.org/10.1038/s41598-017-10665-8, 2017.

Penman, H. L.: I . the Diffusion of Vapours Through, The Journal of Agricultural Science, 30, 437–462, 1940.

Phillips, T. J., Klein, S. A., Ma, H. Y., Tang, Q., Xie, S., Williams, I. N., Santanello, J. A., Cook, D. R., and Torn, M. S.: Using ARM Observations to Evaluate Climate Model Simulations of Land-Atmosphere Coupling on the U.S. Southern Great Plains, Journal of Geophysical Research: Atmospheres, 122, 11,524-11,548, https://doi.org/10.1002/2017JD027141, 2017.

RASMUSSON, E. M.: Atmospheric Water Vapor Transport and the Water Balance of North America, Monthly Weather Review, 96, 720–734, https://doi.org/10.1175/1520-0493(1968)096<0720:awvtat>2.0.co;2, 1968.

Saito, H., Šimůnek, J., and Mohanty, B. P.: Numerical Analysis of Coupled Water, Vapor, and Heat Transport in the Vadose Zone, Vadose Zone Journal, 5, 784–800, https://doi.org/10.2136/vzj2006.0007, 2006.

Shahraeeni, E., Lehmann, P., and Or, D.: Coupling of evaporative fluxes from drying porous surfaces with air boundary layer: Characteristics of evaporation from discrete pores, Water Resources Research, 48, 1–15, https://doi.org/10.1029/2012WR011857, 2012.

Shokri, N., Lehmann, P., and Or, D.: Characteristics of evaporation from partially wettable porous media, Water Resources Research, 45, 1–12, https://doi.org/10.1029/2008WR007185, 2009.

Sun, M. Y., Shi, B., Zhang, C. C., Zheng, X., Guo, J. Y., Wang, Y. Q., He, M. N., and Liu, J.: Quasi-distributed fiber-optic in-situ monitoring technology for large-scale measurement of soil water content and its application, Engineering Geology, 294, 106373, https://doi.org/10.1016/j.enggeo.2021.106373, 2021.

https://doi.org/10.5194/egusphere-2026-1143
Preprint. Discussion started: 6 March 2026


Wang, G., Huang, J., Guo, W., Zuo, J., Wang, J., Bi, J., Huang, Z., and Shi, J.: Observation analysis of land-atmosphere interactions over the Loess Plateau of northwest China, Journal of Geophysical Research Atmospheres, 115, 1–15, https://doi.org/10.1029/2009JD013372, 2010.

Wang, Z., Lei, Y., Che, H., Wu, B., and Zhang, X.: Aerosol forcing regulating recent decadal change of summer water vapor budget over the Tibetan Plateau, Nature Communications, 15, https://doi.org/10.1038/s41467-024-46635-8, 2024.

Weiss, T., Slavík, M., and Bruthans, J.: Use of sodium fluorescein dye to visualize the vaporization plane within porous media, Journal of Hydrology, 565, 331–340, https://doi.org/10.1016/j.jhydrol.2018.08.028, 2018.

Yan, H., Huang, J., He, Y., Liu, Y., Wang, T., and Li, J.: Atmospheric Water Vapor Budget and Its Long-Term Trend Over the Tibetan Plateau, Journal of Geophysical Research: Atmospheres, 125, 1–17, https://doi.org/10.1029/2020JD033297, 2020.

Zhang, M., Wen, Z., Xue, K., Chen, L., and Li, D.: A coupled model for liquid water, water vapor and heat transport of saturated–unsaturated soil in cold regions: model formulation and verification, Environmental Earth Sciences, 75, 1–19, https://doi.org/10.1007/s12665-016-5499-3, 2016.

Zhang, W. and Yao, J.: A fully reconfigurable waveguide Bragg grating for programmable photonic signal processing, Nature Communications, 9, 1–9, https://doi.org/10.1038/s41467-018-03738-3, 2018.

Zhao, Y., Wang, Y., Sun, H., Lin, H., Jin, Z., He, M., Yu, Y., Zhou, W., and An, Z.: Intensive land restoration profoundly alters the spatial and seasonal patterns of deep soil water storage at watershed scales, Agriculture, Ecosystems and Environment, 280, 129–141, https://doi.org/10.1016/j.agee.2019.04.028, 2019.